frontiers | Frontiers in Physics

TYPE Original Research
PUBLISHED 27 November 2024
DOI 10.3389/fphy.2024.1475149

OPEN ACCESS

EDITED BY
Venugopal Rao Soma,
University of Hyderabad, India

REVIEWED BY
Gopala Krishna Podagatlapalli,
Gandhi Institute of Technology and Management (GITAM), India
Moram Sree Satya Bharati,
University of Hyderabad, India

*CORRESPONDENCE
Esteban Builes Münden,
esteban.builes-muenden@tu-braunschweig.de

RECEIVED 02 August 2024
ACCEPTED 29 October 2024
PUBLISHED 27 November 2024

CITATION
Builes Münden E and Dietzel A (2024) Femtosecond laser ablation of nitrocellulose for spatio-temporal flow control in µPADs. *Front. Phys.* 12:1475149. doi: 10.3389/fphy.2024.1475149

Femtosecond laser ablation of nitrocellulose for spatio-temporal flow control in µPADs

Esteban Builes Münden* and Andreas Dietzel

Institut für Mikrotechnik, Technische Universität Braunschweig, Braunschweig, Germany

Microfluidic paper-based analytical devices (µPADs) are gaining popularity due to their low cost and ease of use, but controlling fluid flow for more complex biochemical assays within these devices remains challenging. This study investigates femtosecond laser ablation of nitrocellulose (NC), a preferred material for µPADs, to create mechanically switchable barriers and flow controllers. We investigated NC ablation using single laser pulses and spatially overlapping pulses that generate lines. Single pulse ablation thresholds were determined for wavelengths of 1,030 nm, 515 nm and 343 nm. Line ablation characteristics were investigated as a function of the temporal and spatial pulse separation and laser wavelength. High aspect ratio grooves (up to 4.26) were achieved under specific conditions. These grooves can be used to define the spatial separation of the flow in separated microchannels or to form a barrier line perpendicular to the microchannel that can modulate the temporal behavior of the fluid flow. This barrier introduced an additional high flow resistance slowing down the flow or, if it was designed to cut through nitrocellulose at the entire depth, completely stopped the liquid flow. It was further shown that a barrier formed in this way could be switched by mechanically bending the µPAD at the barrier position. The femtosecond laser patterning method presented here provides precise spatio-temporal control not only for flow branching and multiplexing, but also for controlling flow speed and switching flow on and off within the same manufacturing process. Our results open up new possibilities for complex, multi-step assays on µPADs.

KEYWORDS

FS-laser ablation, nitrocellulose, microfluidic paper-based analytical device (µPAD), fluid flow control, mechanically switchable barrier, ablation threshold, high aspect ratio ablation

1 Introduction

Microfluidic paper-based analytical devices (µPADs) are gaining widespread popularity as detection platforms in medical diagnostics, environmental monitoring, quality assurance and product safety within food production [1, 2]. They rely on materials with hydrophilic micro- or nanopores transporting the fluid to detection zones via capillary action [3, 4]. µPADs offer rapid, reliable and sensitive results using low-cost technologies for the determination or quantification of target analytes in liquid samples [5]. µPADs also demand minimal equipment and training, typically involve a non-complex fabrication,

TABLE 1 Results' compilation from previous studies on the laser ablation characteristics of nitrocellulose, organized chronologically by publication date.

Laser medium	Wave length (λ)	Pulse width (τ)	Ablation threshold (F_{th}, J/cm^2)	Substrate, thickness	Quotation
ArF	193 nm	10 ns	0.020	NC as lacquer, 0.5–3 μm	Deutsch et al. [35] Geis et al. [36]
F_2	157 nm	5 ns	0.025	NC as lacquer, 0.18 μm	Henderson et al. [18]
CO2	10.6 μm	70 ns	3.2	Amersham membrane, 145 μm	Skordoulis et al. [19]
Nd:YAG pulsed	1,060 nm	400 μs	320		
XeCl	308 nm	17 ns	0.185		
XeF	351 nm	30 ns	Between 0.08 and 0.104	NC as lacquer, 1 μm	Furutani et al. [37]

TABLE 2 Ablation threshold values and ablation characteristics for the linear ablation regime following the Lambert-Beer's law at the studied laser wavelengths. Pulse duration was always 212 fs.

Laser wavelength	1,030 nm	515 nm	343 nm
D_p [μm]	34	19	9
F_{th} [J/cm^2]	0.26	0.28	0.03
Precision	4%	12%	7%
Upper limit of the Lambert-Beer's range [J/cm^2]	0.57	0.85	0.75
α_{eff} [mm^{-1}]	27.5	80.0	277.8
Coefficient of determination (R^2)	0.91	0.92	0.85

enable the miniaturization of laboratory procedures, and are portable and disposable [5, 6].

Since the Whitesides group published the first multi-analytical paper-based device in 2007 [7], this field has undergone significant evolution, exploring novel applications and production methods and enhancing control over fluid flow within the system [8]. The complexity of model applications requires automated fluid flow control strategies making use of geometric, mechanical, chemical, electrical, magnetic and thermal approaches [9]. These methods aim to regulate the fluid flow velocity, divert the fluid into different channels or create an externally actuated switchable barrier.

Multi-step assay applications are gaining significant interest in research due to their ability to perform complex tests, such as enzyme-linked immunosorbent assays (ELISA) and polymerase chain reaction (PCR), entirely on a μPAD [10]. These assays require barriers that can be actively switched on and off at desired times, allowing for precise reaction timing and control of assay conditions. Additionally, establishing μPADs with multiparametric measurements or internally calibrated μPADs requires structuring multiple microchannels within the porous material.

Different commercially available materials, including chromatography paper, cellulose membrane or filter paper, have proven their suitability for its use in μPADs [11]. However, the most suitable and reproducible material to be considered in this field is nitrocellulose (NC) [12]. It has already found wide application in commercial rapid tests due to its exceptional protein affinity, its excellent fluid flow properties and its compatibility with a wide range of detection techniques [12].

Nitrocellulose is a polymer produced through the treatment of purified cellulose with nitric acid, leading to the replacement of hydroxyl groups (-OH) on the cellulose glucose rings with nitro groups (-NO2) [13, 14]. The resulting NC possesses dipoles associated with the nitro groups, which interact with the peptide groups of amino acids [12, 15]. This characteristic enhances its protein binding capacity, and consequently, its ability to immobilize antibodies within the matrix, setting it apart from conventional cellulose or cellulose acetate [16]. The pore size, porosity, chemical treatment, thickness and surface quality of the NC membrane are critical parameters that affect the capillary flow, sensitivity and specificity of the μPAD [12, 17].

While the nitro substitution on cellulose enhances its binding capability, it also renders NC explosive, categorizing it as an exothermic material. The explosive characteristics are related to its nitrogen content, which can yield an explosion heat of up to 4586 J/g. Under specific conditions, NC can reach detonation temperatures of up to 3,245°C and detonation velocities of up to 6,300 m/s [14].

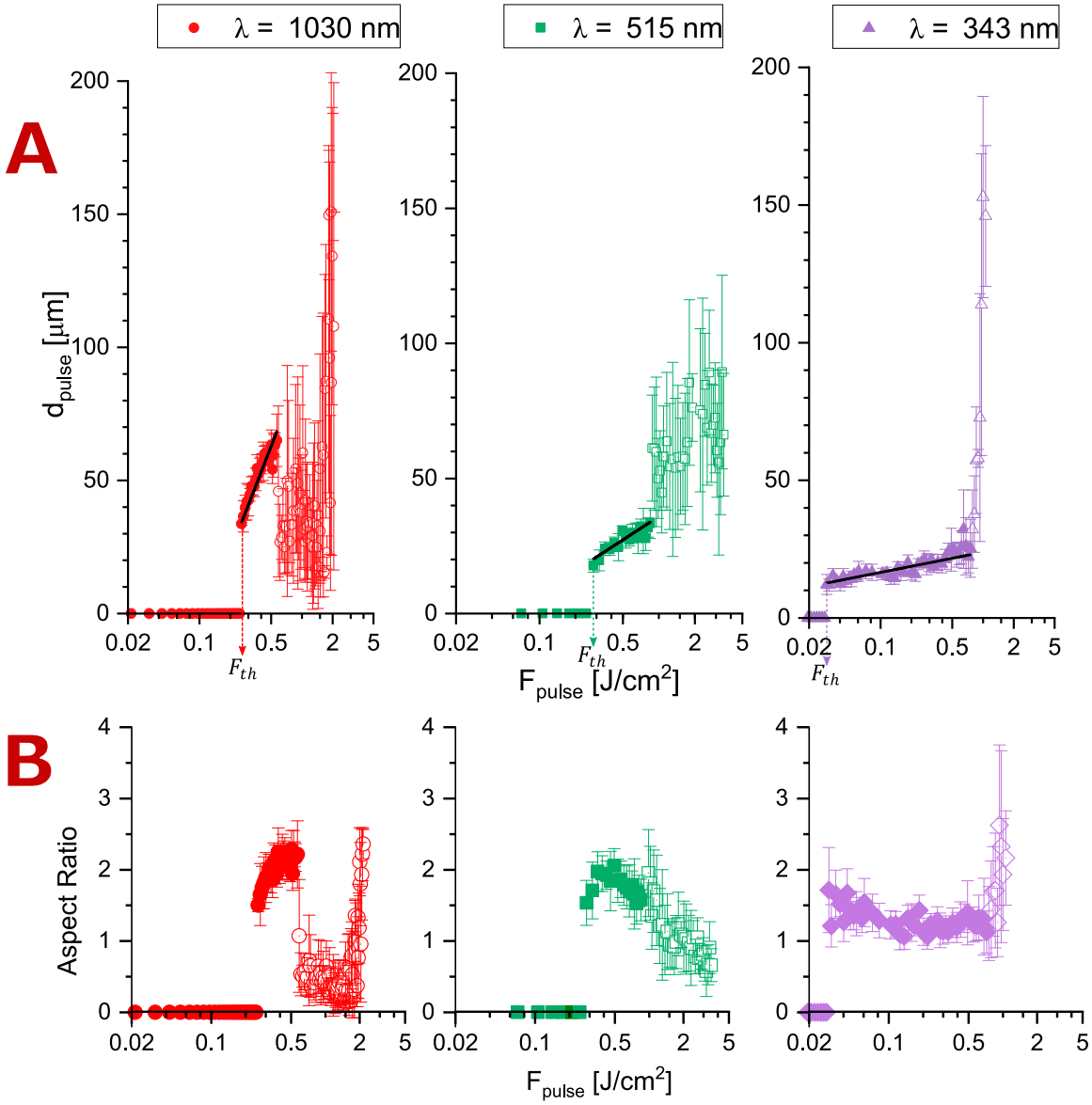

FIGURE 1
Ablation behavior of nitrocellulose subjected to a single pulse at λ = **1,030** nm, λ = **515** nm and λ = **343** nm clearly showing thresholds (indicated by vertical lines. The precise values and their precision are given in Table 2) for fluencies below which no ablation can be observed. Each data point reflects the mean of nine measurements and the error bars reflect the respective standard deviations. Filled datapoints correspond to the linear range (see Figure 2A), not-filled data points above the ablation threshold reflect the appearance of new morphologies at the cavity (see Figures 2B–D). **(A)** Black lines represent the linear approximation in the Lambert-Beer regime. Cavity Depth (d_{pulse}), **(B)** Aspect Ratio of the cavity.

Several authors have explored the phenomenon of ablative photodecomposition of nitrocellulose when exposed to a laser beam. This material was particularly studied as a self-developing photoresist in lithography during the 1980s and 1990s (see summary in Table 1), because it transforms directly into volatile products when exposed to radiation, obviating the necessity for a separate developing step [18]. Most of these studies focused on NC lacquers, which are formulations combining NC with binding agents, like polyurethane (PU) that can be spin-coated on a silicon wafer. These mixtures possess a distinct chemical composition compared to pure NC. Therefore, the only study we are aware of that provides a suitable basis for comparison with our work is the one presented by Skordoulis et al. [19].

Through the interaction of intense laser pulses with the matter, atoms, ions, molecules and clusters are ejected by means of plasma, acoustic shocks and cratering [20]. Such processes were already employed in µPADs for creating separate channels for parallel fluid flow within a device [21–27].

The capability of a laser beam to ablate a material is dependent of its absorption characteristics. The photons are absorbed until a specific depth, described by the Lambert-Beer law [28], which can be formulated for the description of ablation by a single laser pulse as:

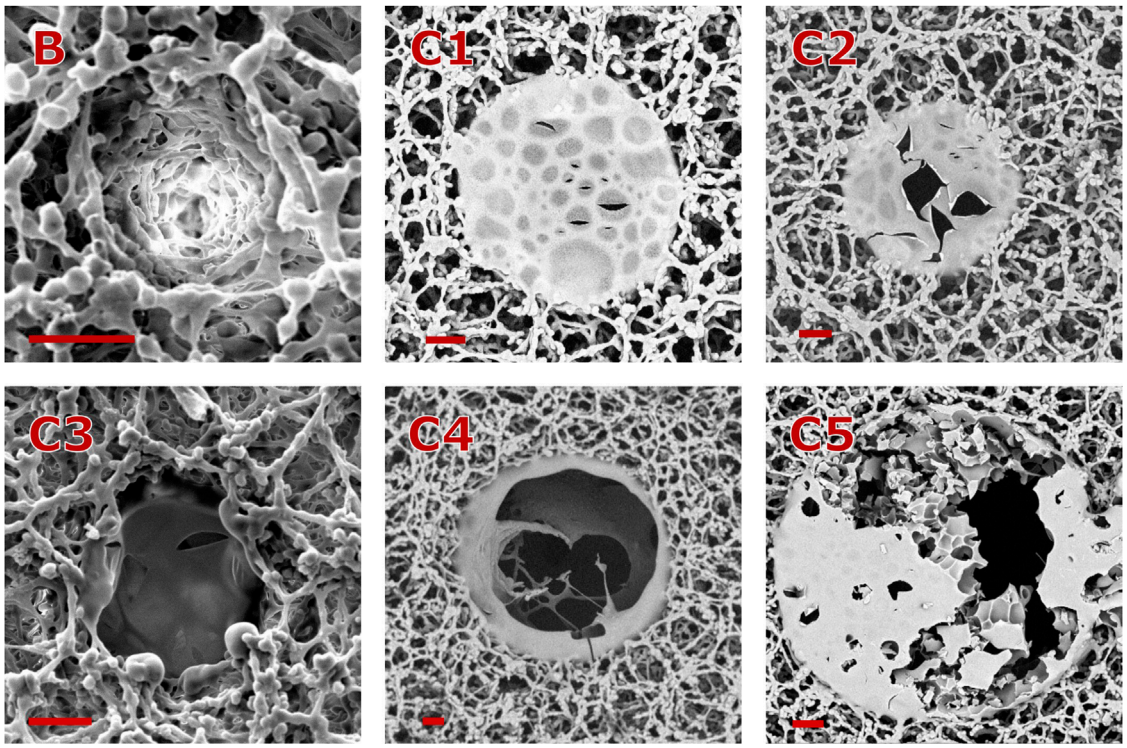

FIGURE 2
Morphologies of cavities ablated with a single pulse. All scale bars represent a distance of **10** µm. **(B)** λ = **515** nm, F_{pulse} = **0.39** J/cm^2; C1: λ = **1,030** nm, F_{pulse} = **0.59** J/cm^2; C2: λ = **1,030** nm, F_{pulse} = **0.62** J/cm^2; C3: λ = **515** nm, F_{pulse} = **1.20** J/cm^2; C4: λ = **343** nm, F_{pulse} = **1.06** J/cm^2; C5: λ = **1,030** nm, F_{pulse} = **1.86** J/cm^2.

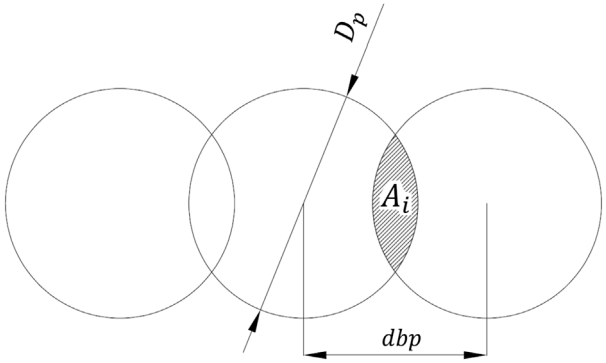

FIGURE 3
Sketch illustrating the pulse overlap definition (***OVL*** = **1.2** in this example).

$$d_{pulse} = \frac{1}{\alpha_{eff}} \cdot \ln\left(\frac{F_{pulse}}{F_{th}}\right)$$

Where d_{pulse} is the depth of the cavity created by the laser pulse, α_{eff} is the linear light absorption coefficient of the material at the laser wavelength, F_{pulse} the fluence delivered by the laser pulse and F_{th} is the threshold fluence which has to be reached to obtain any material ablation.

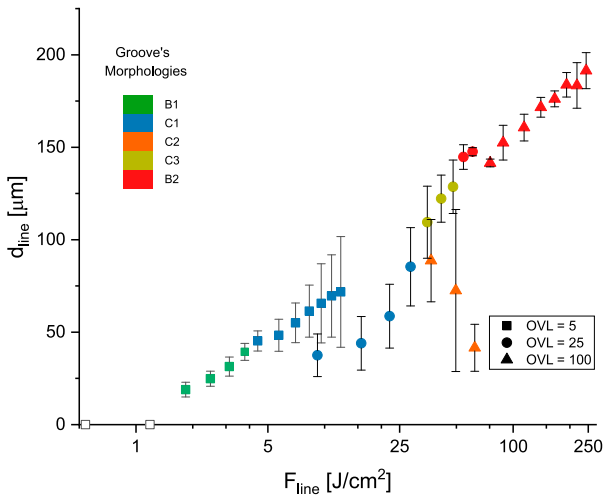

FIGURE 4
Line depth (d_{line}) values obtained with fs-pulses fired at ***f*** = **600** kHz and varied ***OVL*** in dependence of F_{line}. Five different groove morphologies: B, C1, C2, C3 and B2 (see micrographs in Figure 5) were observed.

The precise mechanisms underlying laser ablation, particularly of polymers such as cellulose, remain a subject of ongoing debate within the scientific community [28–30]. There is a

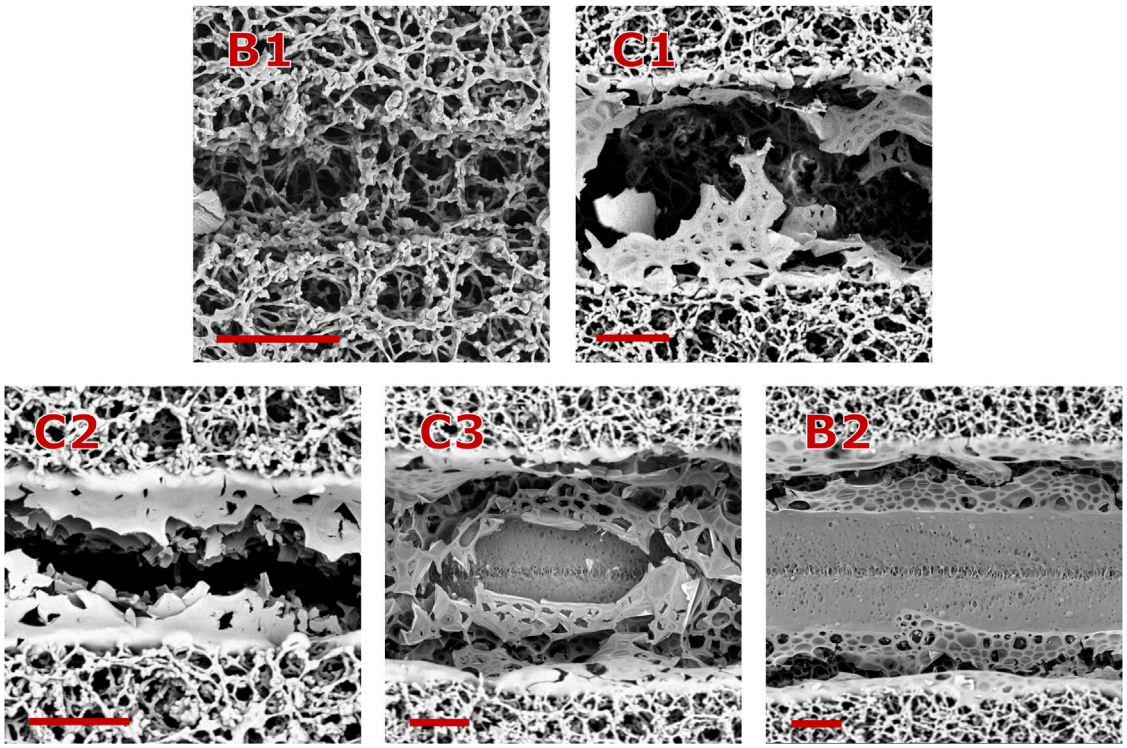

FIGURE 5
Groove morphologies observed at different laser fluences and overlap factors, as shown in Figure 4. For all the cases λ = **1,030** nm and f = **600** kHz. All scale bars represent a distance of **30** µm. B1: ***OVL*** = **5**, F_{line} = **19.1** J/cm^2; C1: ***OVL*** = **5**, F_{line} = **7.0** J/cm^2; C2: ***OVL*** = **100**, F_{line} = **50.0** J/cm^2; C3: ***OVL*** = **25**, F_{line} = **41.5** J/cm^2; B2: ***OVL*** = **25**, F_{line} = **64.3** J/cm^2.

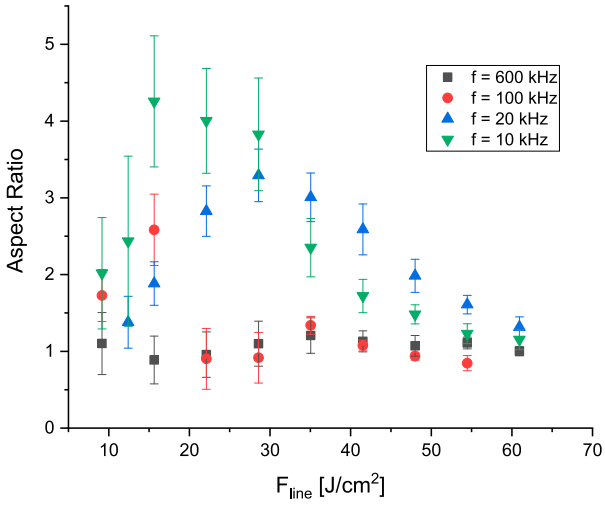

FIGURE 6
Ablated groove aspect ratio for a series of fs-pulses fired at the given repetition rates. ***OVL*** = **25**, λ = **1,030** nm.

general consensus regarding the initial step, which involves the conversion of laser photon energy into electronic excitation, but the subsequent ablation processes include different mechanisms which can be categorized as follows: a) Photothermal ablation: Electronic excitation is rapidly thermalized on a picosecond (ps) timescale, ultimately leading to evaporation. b) Photochemical ablation: Here, electronic excitation directly results in bond breaking. c) Photophysical ablation: This mechanism involves both thermal and non-thermal processes. UV ablation primarily occurs through photochemical ablation, where the material is directly removed by the laser energy. In contrast, IR ablation involves more plasma shielding, which limits direct ablation and increases plasma temperature [31]. Ablation mechanisms depend not only on the laser wavelength but also on the pulse duration. It is known that laser ablation at the ultra-short range possesses unique advantages. These include better controllability and precision in material modification [29], due to minimal heat affected zones, lower ablation threshold fluence and the circumvention of plasma shielding issues [28].

Several works on µPADs have been carried out using laser ablation as fabrication method. The first application dates back to 2013 when Nie et al. [21] successfully optimized a set of parameters for CO_2 laser cutting, enabling precise penetration through the entire depth of a filter paper. Shortly after, Mahmud et al. [22] employed also a CO_2 laser to develop a device using chromatography paper backed on an aluminum foil, achieving a minimum barrier width of 39 ± 15 µm. Kalish et al. [23] also investigated how to control the wicking speed by partially ablating a chromatography paper membrane with a CO_2 laser. Laser ablation has been already implemented for NC structuring in µPAD production [32]. Spicar Mihalic et al. [24] reached a minimum barrier width of 85 ± 5 µm on a 135 µm thick NC membrane using a CO_2

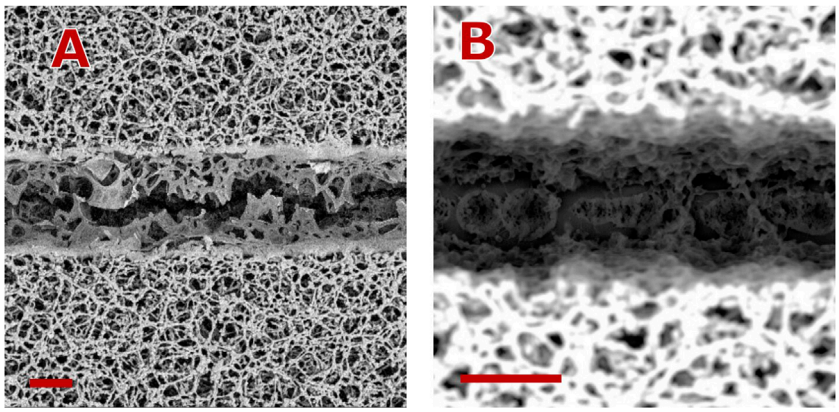

FIGURE 7
Groove morphologies observed at different laser repetition rates. For both cases λ = **1,030** nm, ***OVL*** = **25** and F_{line} = **15.6** J/cm^2. All scale bars represent a distance of **25** µm. **(A)** f = **600** kHz, **(B)** f = **10** kHz.

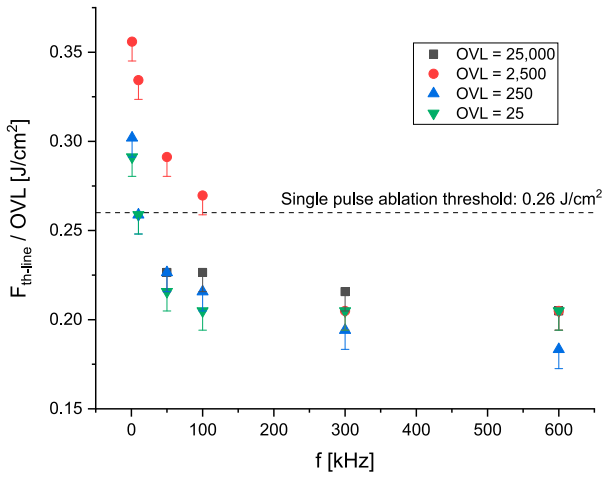

FIGURE 8
Pulse ablation threshold for significant line ablation at different repetition rates and pulse overlaps. For all the cases λ = **1,030** nm.

laser operating at 2 W power and a speed of 11.6 mm/s. Our research group [25, 26] demonstrated ultra-short laser ablation of a NC membrane with a Yb:KGW-solid-state laser emitting at 515 nm wavelength, for use on a multiparametric immunoassay [33]. Sumantakul et al. [27] investigated the NC ablation employing a 455 nm diode laser in enclosed channels using a polyester foil as cover to avoid contamination, minimize evaporative loss, and enhance the chemical stability of chemical reagents on the paper-based device. These studies predominantly focused on finding and optimizing a set of laser parameters for proper µPAD structuring.

In this work, we focus on the easy-to-implement laser-based fabrication of both microchannels and mechanically actuated, robust and reliably switchable barriers in nitrocellulose membranes. Laser ablation was already used for microchannel structuring [21–27], which allows high reproducibility, design flexibility, cost-efficiency, and rapid production. The aim here was to allow the realization of a barrier within the same laser fabrication process, which offers the possibility to effectively stop and restart the fluid flow. Therefore, we investigated how femtosecond laser pulses produced narrow groves that can be used as switchable valves which are initially closed but can be opened at precisely defined time by bending the µPAD at the grove position, which enables the fluid to proceed towards the detection zones.

In order to reach our objective, an in-depth examination of the ablative photodecomposition of a NC membrane under ultra-short pulses that can be specifically used to construct narrow gaps with high aspect ratio reaching the complete depth of the membrane, was carried out. We focused on the ablation behavior when NC is subjected to a single ultra-short laser pulse, and subsequently, we explored how these pulses interact, when they are emitted at a certain repetition rate and with a spatial overlap factor, thereby creating continuous lines. We conducted our study using laser beams with infrared (1,030 nm), visible (515 nm) and ultraviolet (343 nm) light. Moreover, we present the emergence of micro explosions on the NC substrate under specific laser conditions, which had to our knowledge never before been studied in detail.

2 Materials and methods

The ablation process was conducted using a diode pumped Yb:KGW solid-state laser system (Light Conversion Pharos - Vilnius, Lithuania), with an original wavelength $\lambda = 1,030$ nm. We employed a frequency divider with both frequency-doubled ($\lambda = 515$ nm) and frequency-triple ($\lambda = 343$ nm) to investigate the ablation characteristics of nitrocellulose across a wider radiation spectrum. Laser beam profiles and values of spot diameter D_p (defined as D4σ) were measured for $\lambda = 1,030$ nm and $\lambda = 515$ nm using a laser beam analyzer composed from a beam splitter (LBS-300) and a beam profiling camera (BGS-USB-SP928-OSI from Ophir-Spiricon, LCC - North Logan, United States). Beam profiles were analyzed using the software BeamGage Standard (Ophir Optronics, Jerusalem). D_p for $\lambda =$ 343 nm laser beam was determined indirectly. A glass wafer

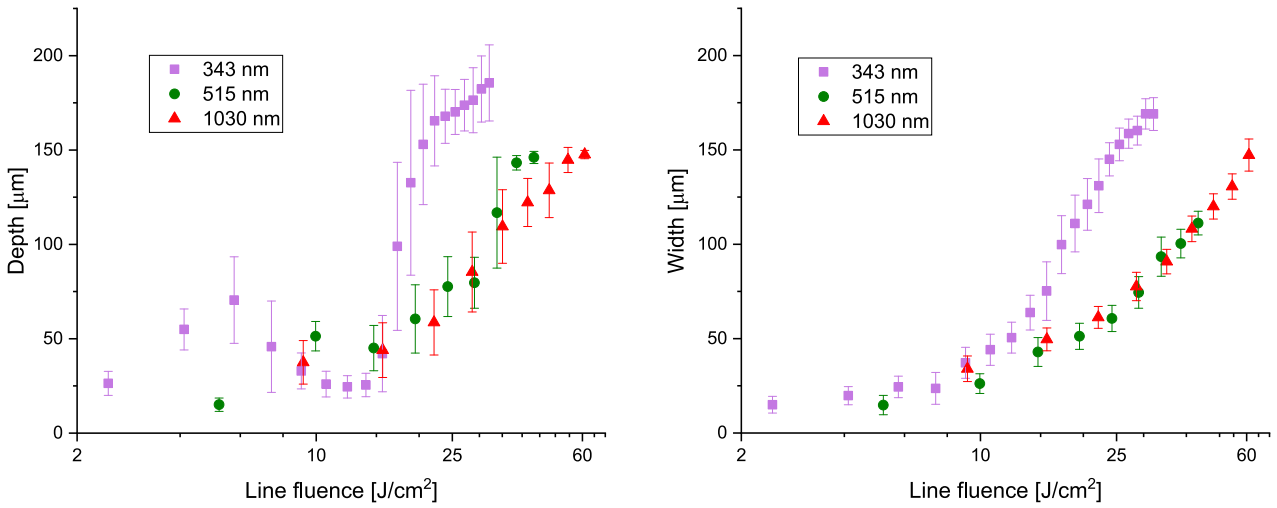

FIGURE 9
Ablated groove depth and width for a series of fs-pulses fired at the given laser wavelengths. ***OVL*** = **25**, ***f*** = **600** kHz.

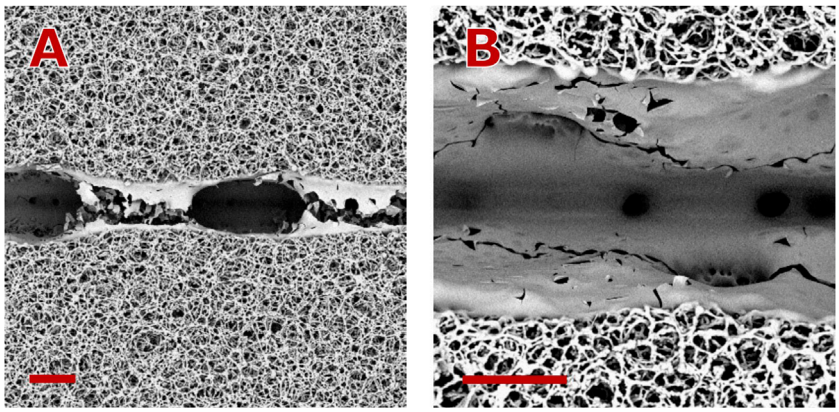

FIGURE 10
Particularities of the groove ablation at λ = **343** nm. For both cases, ***OVL*** = **25**, ***f*** = **600** kHz. All scale bars represent a distance of **50** µm. **(A)** Nitrocellulose layers as observed in Figure 5C are partially ablated. F_{line} = **15.6** J/cm^2. **(B)** Accelerated polyester ablation. F_{line} = **22.3** J/cm^2.

was coated with a 200 nm Chromium layer and subsequently subjected to laser pulses near the ablation threshold (Pulse energy E_p = 0.1 µJ). The laser spot diameter D_p was defined as the average obtained from nine single pulse experiments. Values for D_p of 34 µm for λ = 1,030 nm, 19 µm for λ = 515 nm, and 9 µm for λ = 343 nm were determined. Laser beam ablation experiments were carried out on a micro-structuring platform (Microstruct-C from 3DMicromac, Germany). The beam was focused using a sensor head (Keyence LK-G010) positioning the scanner lens on focus with an accuracy of 0.02 µm. This sensor uses the laser triangulation method to detect the reflection of the nitrocellulose membrane surface and determine the focus position. Pulse energies were measured using a power sensor (UP19K-15S-W5-XT-3DM Power Detector from Gentec-EO, Inc., Canada). The laser beam's position on the membrane surface was controlled in the case of λ = 1,030 nm and λ = 515 nm by a high-performance 3D scanner (Scanlab RTC 5), facilitating high processing speeds. In the case of λ = 343 nm, a fixed objective was used in combination with the computer motorized stage of the micro-structuring platform. Pulses with durations of 227 fs and 212 fs were emitted at repetition rates f = 100 kHz and f = 600 kHz, respectively.

Nitrocellulose membranes (Unisart® CN 140 Backed from Sartorius, Göttingen, Germany) with a nominal thickness ranging from 225 to 255 µm and a precise amount of anionic surfactant for fast wetting characteristics were used [34]. These membranes included a polyester clear support and the capillary speed was specified as 95–155 s/40 mm. NC membranes were reinforced with a backing card (0.01″ White Polystyr. w/KN-2211® from KENOSHA B.V., Netherlands). Characterization of ablation results was carried out using a laser scanning microscope (Keyence VK-X260) and a desktop SEM (Phenom XL, ThermoFisher Scientific, United States).

For the barrier proof of concept, 10% Fetal Bovine Serum (Sigma Aldrich, Germany) in PBS was used in all cases as fluid.

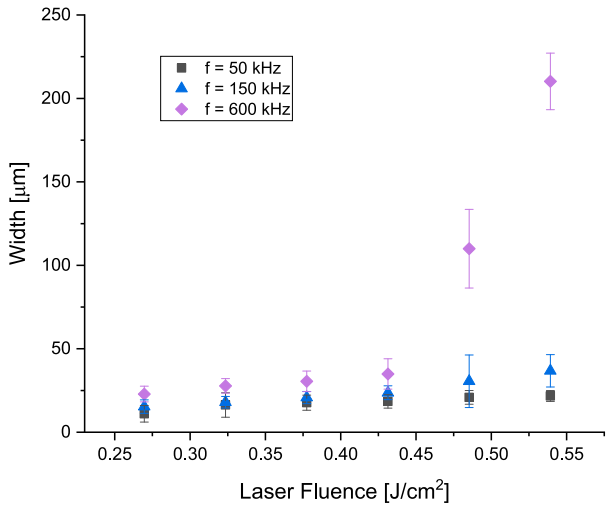

FIGURE 11
Channel width for λ = **1,030** nm, ***OVL*** = **3000** and the given pulse repetition rate. Sudden increase in groove width and its related error bars signaling explosions expanding transversal to the groove direction.

3 Results

3.1 Single pulse ablation

Single laser pulses at $\lambda = 1,030$ nm, $\lambda = 515$ nm and $\lambda = 343$ nm with a pulse width of 212 fs were focused on the NC membrane using E_p between 0.1 µJ and 20 µJ for $\lambda = 1,030$ nm, 0.1 µJ and 10 µJ for $\lambda = 515$ nm, and 0.002 and 1.320 µJ for $\lambda = 343$ nm. The ablation depth d_{pulse} was determined as the average difference between the average height of the surrounding nitrocellulose and the minimum height in the ablated cavities for nine different pulses. The removal threshold fluence F_{th} was considered to be exceeded as soon as a removal depth that differed significantly from the surface roughness of the nitrocellulose material could be determined. Values obtained for F_{th} are given in Table 2. The given precision values represent the relative deviation between F_{th} and the highest laser fluence tested that did not result in significant ablation. For verification, 30 pulses with laser fluences just below F_{th} were delivered at the same position with $f = 1$ Hz and no significant ablation was observed. Results for d_{pulse} and aspect ratio of the cavity in dependence of the delivered single pulse laser fluence F_{pulse} are given in Figure 1. Aspect ratio was defined as the relation between d_{pulse} and cavity diameter.

With help of SEM micrographs (see Figure 2) three different morphological regimes were identified:

A. No-ablation regime below the ablation threshold.
B. Lambert-Beer regime directly above F_{th}. At all the studied laser wavelengths a linear relationship between F_{pulse} and d_{pulse}, consistent with the Lambert-Beer's law was found. Coefficients of determination for linear logarithmic interpolation, the resulting linear absorption coefficients and values for the upper limit of this regime are given in Table 2. This regime is associated with an ablation morphology as illustrated in Figure 2B. It shows that material is ejected with minimal modification of area surrounding the cavity. As F_{pulse} increases, there is a growing tendency for melting at the rim of the cavity, resulting in smoother sidewalls.
C. Scatter regime just above the Lambert-Beer regime when F_{pulse} has reached the critical values 0.57 J/cm^2 for $\lambda = 1,030$ nm and 0.85 J/cm^2 for $\lambda = 515$ nm. Here a lid in form of a thin film out of NC has formed. For infrared irradiation ($\lambda = 1,030$ nm), this film appears near the NC surface (see Figure 2C1) and can fracture due to mechanical or thermal instabilities, as shown in Figure 2C2. Consequently, values for d_{pulse} measured by means of a laser scanning microscope are significantly reduced and show notable uncertainties. When employing visible light irradiation ($\lambda = 515$ nm) this film appears lower than the NC surface (see Figure 2C3) and a deeper cavity compared to $\lambda = 1,030$ nm is measured. For UV irradiation ($\lambda = 343$ nm) this regime starts upon reaching $F_{pulse} = 0.75$ J/cm^2 when complete removal of the nitrocellulose membrane is observed and the polyester layer below starts to be ablated (see Figure 2C4). At $\lambda = 1,030$ nm a somewhat deviating morphology was observed for values of $F_{pulse} > 1.68$ J/cm^2, but not in every case. The nitrocellulose ejected by ablation clusters on the membrane surface and generates a thicker non-uniform layer, as shown in Figure 2C5. It can be assumed, that the persistence of this layer depended strongly on the local conditions in the stochastic nitrocellulose material. Because of the difficulty in determining d_{pulse} due to the partial formation of a lid capping the ablation cavity, this regime is characterized by a much larger measurement scatter, which led us to call it the scatter regime.

3.2 Line ablation

For the ablation with spatially overlapping pulses, we introduced the parameter *OVL*. It is a measure of the degree of overlap of subsequent laser pulses with the area of the initial individual pulse as defined by D_p. *OVL* is calculated as:

$$\boldsymbol{OVL} = \frac{1}{\pi \cdot \left(\frac{D_p}{2}\right)^2} \cdot \sum_i \boldsymbol{A_i}$$

where A_i is the areal overlap of each pulse $i = 0, 1, 2, 3\ldots$ with the area of a first laser pulse ($i = 0$) as sketched in Figure 3. The values for A_i were calculated using a Matlab program in dependence of laser scanning speed v and pulse repetition rate f. Only values for $dbp \leq D_p$ had to be considered in the summation, with $\boldsymbol{dbp} = \frac{v}{f}$.

In this work, we studied the influence of three important parameters on the characteristics of an ablated line: the spatial density of laser pulses quantified by *OVL*, the temporal pulse density quantified by the repetition rate f, and the laser wavelength λ.

3.2.1 Influence of the spatial pulse separation given by *OVL*

Lines were ablated at $\lambda = 1,030$ nm, $f = 600$ kHz and a pulse duration of 212 fs. v was adjusted to achieve *OVL* values of 5, 25 and 100. Subsequently, the resulting lines were measured using laser scanning microscope at a 20X magnification. The obtained topography image, consisting of 1,024 × 768 pixels, was analyzed

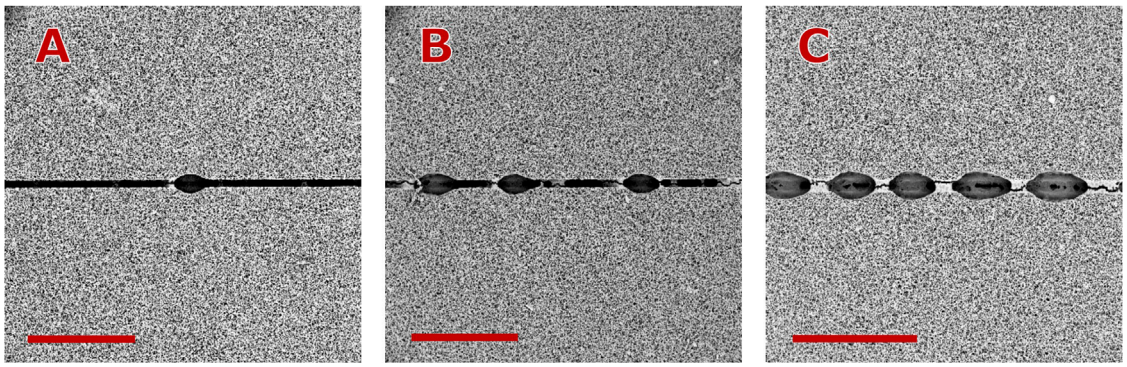

FIGURE 12
Appearance of macro-explosions on the ablated nitrocellulose at high overlap factors. In all cases ***OVL*** = **3000**, λ = **1,030** nm, ***f*** = **600** kHz. Scale bars represent a distance of 500 µm. **(A)** F_{line} = **1341** J/cm^2, **(B)** F_{line} = **1395** J/cm^2, **(C)** F_{line} = **1446** J/cm.^{2}.

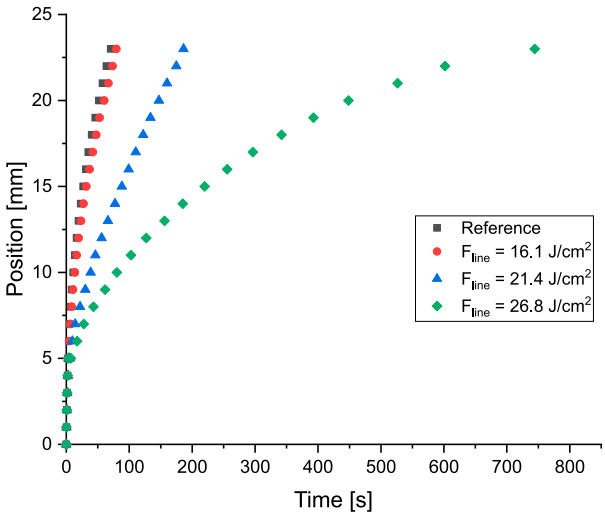

FIGURE 13
Modification of the fluid flow behavior by ablation of a line at the position of 5 mm. In all the cases ***OVL*** = **5**, λ = **1,030** nm, ***f*** = **10** kHz and F_{line} as given in the graphic. Reference refers to no ablated line.

using a Matlab code. This code determined the positions of the groove (ablated line) edges to calculate its width and the deepest point in 1,024 linear depth profiles perpendicular to the groove. This procedure was repeated three times to ensure robust and reliable data for the widths and depths of the ablated lines. The laser fluence for line ablation was calculated as $\boldsymbol{F_{line} = F_{pulse} \cdot OVL}$, where F_{pulse} represents the single pulse fluence. Line depth d_{line} as function of F_{line} is given in Figure 4. Moreover, five different groove morphologies were observed at different laser parameter sets, as illustrated in Figure 5, which can be grouped in the following regimes:

A. No-ablation regime for F_{line} < 1.8 J/cm^2 (in all tested OVL s).
B. Linear regime observed:
   1. At OVL = 5, with 1.8 J/cm^2 ≤ F_{line} ≤ 12.2 J/cm^2. A linear Lambert-Beer relation was obtained (R^2 = 0.99, $\alpha_{eff-line}$ = 34.8 mm^{-1}). For 1.8 J/cm^2 ≤ F_{line} ≤ 4.4 J/cm^2, grooves exhibited a consistent depth profile along the complete line length, which is corroborated by the relatively small error bars for d_{line}. The ablation impact on the surrounding areas was minimal to non-existent, as exemplary shown in Figure 5B1. For 4.4 J/cm^2 < F_{line} ≤ 12.2 J/cm^2, linearity was conserved, but a different groove morphology was observed, as described under C1.
   2. At OVL = 25, and OVL = 100 with F_{line} ≥ 60.2 J/cm^2, d_{line} was also found to be linear related to F_{line} (R^2 = 0.95, $\alpha_{eff-line}$ = 30.3 mm^{-1}). In this morphology, the NC membrane is in the middle of the grove ablated through its entire depth, exposing the polyester over all the groove length (see Figure 5B2). An increment of F_{line} at those conditions generates solely polyester ablation. No thin film lids were observed. This process leads to low uncertainties (scatter) in the measuring of d_{line}.

C. Scatter regime, where three sub-morphologies were found:
   1. At ***OVL*** = 25, with **5.7 J/cm^2** ≤ $\boldsymbol{F_{line}}$ ≤ **28.6 J/cm^2**, a new morphology emerged. A first single pulse creates a lid in form of a thin film near the surface of the NC, and subsequent pulses only partially ablate this film. This process leads to higher uncertainties (scatter) in the measuring of $\boldsymbol{d_{line}}$ (see Figure 5C1).
   2. At OVL = 100, with 36.7 J/cm^2 ≤ F_{line} ≤ 62.6 J/cm^2, a modification to the previous sub-morphology was observed. Several lid layers were formed over the entire depth of the groove instead of a single layer (see Figure 5C2). This process also leads to high uncertainties (scatter) in the measuring of d_{line}.
   3. At OVL = 25, with 35.0 J/cm^2 ≤ F_{line} ≤ 45.5 J/cm^2, the nitrocellulose membrane was partially ablated through its entire depth, exposing the underlying polyester (see Figure 5C3). Any thin film lids that may have been formed after initial pulses in this region are completely removed by subsequent overlapping pulses. This process leads to less uncertainties (scatter) in the measuring of d_{line}

TABLE 3 Consistency of the results for fluid flow behavior by partial ablation of a line at a given position.

Single pulse energy, µJ	Line fluence, J/cm^2	Ablated width, µm	Time required to overcome the ablated zone, s	Time required to reach the benchmark of 23 mm, s
0 (Reference)	-	-	-	65.3 ± 6.7
30	16.1	80.5 ± 9.4	0.6 ± 0.0	76.0 ± 10.0
40	21.4	100.3 ± 8.0	2.5 ± 1.1	191.5 ± 56.1
50	26.8	117.3 ± 10.1	3.6 ± 0.5	741.3 ± 4.3

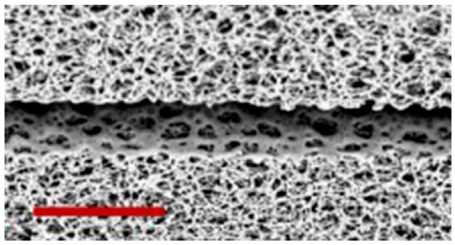

FIGURE 14
SEM micrograph of the developed barrier, as given in Table 4. Scale bar represent a distance of 80 µm.

TABLE 4 Laser parameter sets for barrier gap removal.

	Coarse removal	Fine removal
λ, nm	1,030	343
F_{th}, J/cm^2	0.26	0.03
OVL	5	25
F_{line}, J/cm^2	4.29	0.25
f, kHz	10	10
Depth achieved, µm	99.99 ± 3.20	20.58 ± 2.88
Width achieved, µm	39.74 ± 1.68	9.72 ± 1.57
Repetitions	1	3

The groove aspect ratio (d_{line} over groove's width) was found to be not directly affected by OVL nor by F_{line} under the studied circumstances. Average aspect ratio of all the data presented in Figure 4 was calculated as 1.04 ± 0.22.

3.2.2 Influence of the temporal pulse separation given by *f*

An external electro-optical pulse picker based on a Pockels cell was used to convert the original laser's pulse repetition rate of $f = 600$ kHz into $f = 100$ kHz, $f = 20$ kHz and $f = 10$ kHz. Laser mark speeds were adjusted to achieve in all cases an overlap factor $OVL = 25$. d_{line} and groove aspect ratio were studied.

While the depth of the ablated lines (d_{line}) was found to be independent of the laser frequency, their aspect ratio was found to be dependent on both the laser frequency and the line fluence. Generally, an aspect ratio of 1 was obtained at $f = 600$ kHz and $f = 100$ kHz. However, when the temporal pulse separation was increased by decreasing f to 10 kHz and 20 kHz, high aspect ratio grooves of up to 4.26 were observed (see Figure 6). This difference in groove aspect ratio is attributed to lid effects (as shown for single pulses in Figure 2). The lid formation in line patterning with overlapping pulses depends on the time difference between single pulses. Figure 7 shows two groove morphologies for lines structured at $\lambda = 1,030$ nm, $OVL = 25$ and $F_{line} = 15.6$ J/cm^2. With a 1.7 µs time difference between pulses ($f = 600$ kHz, as shown in Figure 7A), nitrocellulose builds lids on the groove, preventing sufficient depth. In contrast, a 100 µs time difference between pulses ($f = 10$ kHz, as shown in Figure 7B) creates grooves without lids that are ablated partially until the polyester ground.

It remains to be clarified whether the Labert-Beer Law can be extended to describe line ablation processes as $\boldsymbol{d_{line} = \frac{1}{\alpha_{eff}} \cdot \ln\left(\frac{F_{line}}{F_{th}}\right)}$. Additionally, it is uncertain if the fluence threshold for line ablation ($F_{th-line}$) is the same as for single pulses (F_{th}), or if this threshold depends on the spatial pulse separation (given by OVL) and the temporal pulse separation (given by f).

Line ablation thresholds for NC were investigated for overlap factors (OVL) between 25 and 25,000 and repetition rates (f) between 1 kHz and 600 kHz. As illustrated in Figure 8, pulse fluences for line ablation thresholds ($F_{th-line}/OVL$) were found to exceed the single pulse ablation threshold ($F_{th} = 0.26$ J/cm^2) for larger OVL values combined with lower f values. This suggests that fluence contributions from different femtosecond pulses can accumulate when delivered within a sufficiently short time interval (approximately 10 µs to 1 ms). For extremely short time intervals (below 10 µs), line ablation was achieved with pulse fluences below the single pulse fluence threshold. This indicates that the ablation effect of multiple pulses is even stronger compared to single pulses of equivalent total fluence. In these cases, ablation may not begin with the initial laser pulse but requires multiple lower fluence pulses, a phenomenon known as incubation. This process involves physical or chemical changes in the material induced by the first few laser pulses, which often lead to increased absorption at the irradiation wavelength [28].

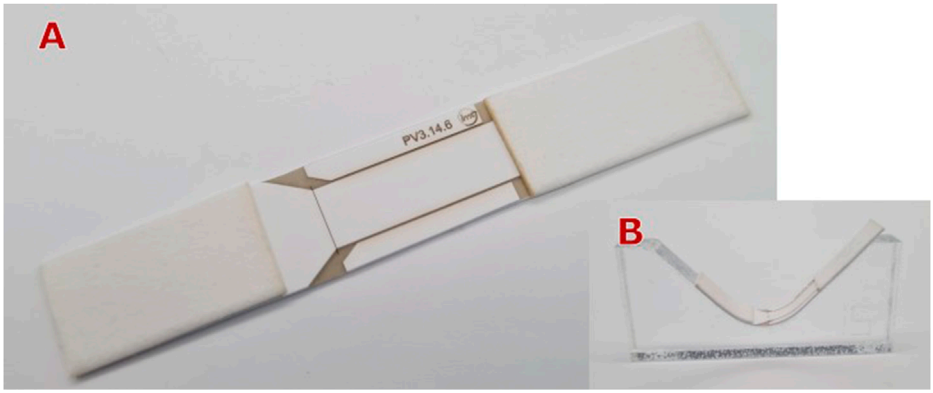

FIGURE 15
(A) Mechanical actuated barrier by bending it at the gap region, **(B)** Template used for achieving a specific bending radius.

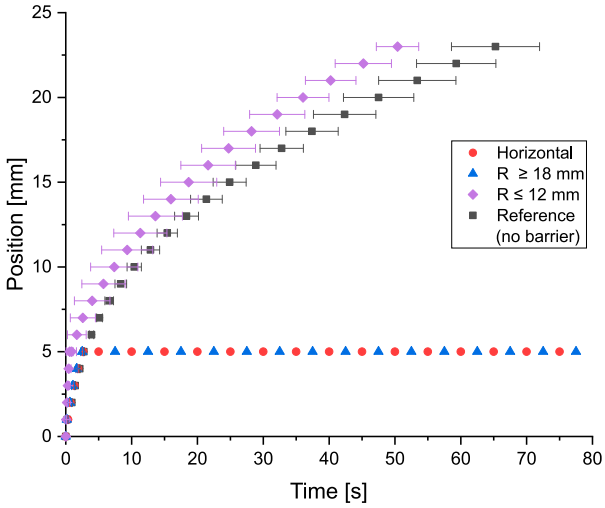

FIGURE 16
Functionality of the mechanically actuated barrier. Testing the μPAD without bending it (horizontal position) shows that the flow stops at the barrier position of 5 mm. The same behavior is observed when the μPAD is bent at the gap position with bending radii of 18 mm or greater. For bending radii of 12 mm or smaller, the barrier was actuated in all cases. The higher fluid flow velocity respect to the reference value at the bent position can be attributed to inertial forces due to the position of the paper stripe on the template. Six tests were conducted for each data series.

3.2.3 Influence of the laser wavelength (λ)

Laser pulses at $\lambda = 1{,}030$ nm, $\lambda = 515$ nm and $\lambda = 343$ nm were delivered using a frequency divider. Pulses were emitted at $f = 600$ kHz and an $OVL = 25$ was achieved in all cases by adjusting v. Achieved groove's depth and width are depicted in Figure 9.

When employing visible light irradiation at $\lambda = 515$ nm, groove morphologies were found to be the same as described at IR irradiation at $\lambda = 1{,}030$ nm. Groove width and depth dimensions showed to be similar in both cases.

Ultraviolet irradiation at $\lambda = 343$ nm however showed different ablation regimes. A first linear regime induces the creation of grooves without impacting the surrounding areas at 2.5 J/cm^2 $\leq F_{line} \leq$ 5.8 J/cm^2. The linear behavior between laser fluence and ablated depth established under these conditions is disrupted at higher fluences by the emergence of multiple nitrocellulose layers, as illustrated in Figure 5C2. By $F_{line} = 14.0$ J/cm^2, partial ablation of the generated nitrocellulose layers becomes feasible, as depicted in Figure 10A. Beyond $F_{line} = 20.6$ J/cm^2, grooves were ablated across all the nitrocellulose. In this case, the underlaying polyester layer experienced accelerated etching (see Figure 10B), a phenomenon similar to what is observed by single pulse ablation.

3.2.4 Special case: nitrocellulose explosion phenomenon

Grooves were ablated using a laser beam with $\lambda = 1{,}030$ nm, emitting at repetition rates of 600 kHz, 150 kHz and 50 kHz, with a pulse duration of 212 fs. Laser mark speeds were adjusted to achieve an overlap factor of $OVL = 3000$, while laser pulse fluences were varied between $F_{pulse} = 0.214$ J/cm^2 and $F_{pulse} = 0.536$ J/cm^2.

When employing low laser mark speeds, resulting in high overlap factors (such as 3000 in this instance), an ablation phenomenon revealing the explosive nature of nitrocellulose becomes evident. Specially at high repetition rates, explosions visible to the naked eye appeared transversally to the length of the ablated groove (see Figures 11, 12). Detailed analysis under an electron microscope reveals that in all cases where these explosions occur, the polyester layer is reached.

3.3 Proof of concept for active valving

High aspect ratio ablation assures that the width of the valving gap can be minimized. Two applications were developed for fluid flow control based on the ablation characteristics discussed earlier. The first one reduces the fluid flow velocity after integrating an ablated line perpendicular to the flow direction. The second one uses

different laser parameters to achieve ablation of nitrocellulose over the entire membrane depth, successfully stopping the flow until the device is mechanically actuated by bending.

Fluid flow behavior was affected by additional fluidic resistance at the ablated region due to partial ablation of the nitrocellulose membrane. Partial ablation refers to the creation of gaps that do not penetrate the entire depth of the nitrocellulose membrane, resulting in increased fluidic resistance in the ablated region. Line fluences were adjusted to $F_{line} = 16.1$ J/cm^2, $F_{line} = 21.4$ J/cm^2 and $F_{line} = 26.8$ J/cm^2. A laser beam with $\lambda = 1{,}030$ nm was employed, emitting at $f = 10$ kHz and with $OVL = 5$. At $F_{line} = 16.1$ J/cm^2, the partial ablation resulted in a moderate increase in fluidic resistance, causing a slight retardation in fluid flow across the μPAD. As F_{line} increased, a more pronounced effect on fluid flow was observed, with a significant reduction in flow rate through the μPAD. Exemplary graphics for the fluid flow behavior at the given line fluences are shown in Figure 13. The consistency of the results is shown in Table 3.

In a second application, nitrocellulose ablation over the entire membrane depth was achieved using two parameter sets: One for high-speed course removal and one for low-speed fine removal. These parameters were selected for the NC removal on the gap region.

In the first step, high etching rates were targeted. The laser wavelength was set to $\lambda = 1{,}030$ nm, and the groove characteristics were chosen within the linear range (groove morphology described by Figure 5B1, 1.3 J/cm^2 $\leq F_{line} \leq$ 4.4 J/cm^2), using $OVL = 5$. High aspect ratio removal was achieved with $f = 10$ kHz.

In the second step, line fluence was set below the ablation threshold of the polyester backing to ensure selective ablation of the NC membrane. This approach minimizes energy input and prevents the formation of a polyester layer on the groove walls. Maintaining only NC on the walls is crucial, as it prevents undesired fluidic resistance when the gap is closed. UV Laser (λ = 343 nm) was used due to the significantly lower nitrocellulose ablation threshold compared to visible and IR ranges. The line polyester ablation threshold at $\lambda = 343$ nm, $OVL = 25$ and $f = 10$ kHz was determined to be $F_{line-th} = 2.52$ J/cm^2. This threshold was determined using the same method as for the nitrocellulose line ablation threshold. Figure 14 shows a SEM micrograph of the developed barrier, revealing partial condensation of NC over the groove wall. Specific laser beam parameters are detailed in Table 4.

The mechanical actuated barrier is depicted in Figure 15A. Barrier actuation was tested both at the horizontal position and by bending it using templates with arc radii between 5 mm and 240 mm (see Figure 15B). Testing the μPAD at the horizontal position (no bending), results in a completely stop of the flow at the gap position of 5 mm–It means, the barrier was completely closed. This condition was also maintained when the μPAD was tested on templates with bending radii of 18 mm or greater. Using a bending radius of 15 mm as template, a flow bridging rate of 33% was observed for six tests. When using a template with bending radius of 12 mm or smaller, the barrier was actuated in all the cases. Figure 16 shows the fluid flow behavior for the μPAD at the given bending radii.

4 Conclusion

This study demonstrates the potential of femtosecond laser ablation for precise fluid flow control in nitrocellulose membranes for μPADs, enabling both flow velocity modulation and mechanically switchable barriers. By investigating ablation characteristics across multiple wavelengths and laser configurations, we have identified optimal parameters for producing narrow, high aspect ratio barriers that can effectively control fluid flow.

Our findings significantly advance the understanding of laser ablation in nitrocellulose membranes, particularly when compared to previous literature. The observed ablation thresholds for a single pulse ($F_{th} = 0.26$ J/cm^2 at $\lambda = 1{,}030$ nm, $F_{th} = 0.28$ J/cm^2 at $\lambda = 515$ nm, and $F_{th} = 0.03$ J/cm^2 at $\lambda = 343$ nm) are notably lower than previous reports [19], which can be attributed to several factors, primarily the pulse duration. Our investigation also provides valuable insights into the interaction between overlapped ultra-short laser pulses and the nitrocellulose membranes, contributing to a deeper understanding of the ablation process and offering guidance for fine-tuning laser parameters to achieve desired barrier properties.

The investigation of laser-nitrocellulose interactions provides the foundation for developing μPAD valves that can be easily integrated into μPAD manufacturing processes. We engineered two types of control devices:

1. Flow Velocity Modulation–A device, incorporating a partially-ablated line perpendicular to the fluid flow demonstrated significant flow retardation. The time required for fluid to traverse an 18 mm benchmark after contact with the line, increased from 10.7 s to 675.7 s, correlating with increasing laser line fluence. This retardation offers the possibility to increase the fluid residence time at test and/or control zones.
2. Mechanically Actuated Barrier–We fabricated a device featuring a laser-ablated gap that completely halts fluid flow. Upon mechanical actuation (bending it with a radius ≤ 12 mm at the gap region), fluid flow resumes. This switchable barrier enables on-demand flow control, critical for multi-step assays.

These innovations in fluid dynamics control enhances μPAD functionality and versatility, facilitating more complex, multi-step analytical procedures.

Future work should focus on optimizing the mechanical actuation of these laser-ablated barriers and exploring their performance in various μPAD applications. Additionally, further investigation into the long-term stability and reliability of these barriers under different environmental conditions would be valuable for practical implementation.

Overall, this study represents a significant step forward in μPAD fluid control techniques, offering new possibilities for a wider use in more sophisticated analytical applications that require controllable flow.

Data availability statement

The raw data supporting the conclusions of this article will be made available by the authors, without undue reservation.

Author contributions

EBM: Conceptualization, Data curation, Formal Analysis, Investigation, Methodology, Project administration, Software, Supervision, Validation, Writing–original draft, Writing–review and editing. AD: Conceptualization, Funding acquisition, Supervision, Writing–original draft, Writing–review and editing.

Funding

The author(s) declare that financial support was received for the research, authorship, and/or publication of this article. This study was founded by the AiF (Arbeitsgemeinschaft industrieller Forschungsvereinigungen) - IGF, Project Nr. 20949 N.

Acknowledgments

We would like to express our sincere gratitude to Daniel Gustavo Montenegro Rodríguez and Rokas Kazlauskas for their invaluable assistance with the measurements conducted for this study.

Conflict of interest

The authors declare that the research was conducted in the absence of any commercial or financial relationships that could be construed as a potential conflict of interest.

The author(s) declared that they were an editorial board member of Frontiers, at the time of submission. This had no impact on the peer review process and the final decision.

Publisher's note

References

1. Koczula KM, Gallotta A. Lateral flow assays. *Essays Biochem* (2016) 60(1):111–20. doi:10.1042/ebc20150012

2. Yang Y, Noviana E, Nguyen MP, Geiss BJ, Dandy DS, Henry CS. Paper-based microfluidic devices: emerging themes and applications. *Anal Chem* (2017) 89(1):71–91. doi:10.1021/acs.analchem.6b04581

3. Berli CLA, Kler PA. A quantitative model for lateral flow assays. *Microfluid Nanofluid* (2016) 20(7):104–9. doi:10.1007/s10404-016-1771-9

4. Washburn EW. The dynamics of capillary flow. *Phys Rev* (1921) 17(3):273–83. doi:10.1103/physrev.17.273

5. Posthuma-Trumpie GA, Korf J, van Amerongen A. Lateral flow (immuno)assay: its strengths, weaknesses, opportunities and threats. A literature survey. *Anal Bioanal Chem* (2009) 393(2):569–82. doi:10.1007/s00216-008-2287-2

6. Ngom B, Guo Y, Wang X, Bi D. Development and application of lateral flow test strip technology for detection of infectious agents and chemical contaminants: a review. *Anal Bioanal Chem* (2010) 397:1113–35. doi:10.1007/s00216-010-3661-4

7. Martinez AW, Phillips ST, Butte MJ, Whitesides GM. Patterned paper as a platform for inexpensive, low-volume, portable bioassays. *Angew Chem Int Ed Engl* (2007) 46(8):1318–20. doi:10.1002/anie.200603817

8. Han T, Jin Y, Geng C, Aziz AR, Zhang Y, Deng S, et al. Microfluidic paper-based analytical devices in clinical applications. *Chromatographia* (2020) 83(6):693–701. doi:10.1007/s10337-020-03892-1

9. Modha S, Castro C, Tsutsui H. Recent developments in flow modeling and fluid control for paper-based microfluidic biosensors. *Biosens Bioelectron* (2021) 178:113026. doi:10.1016/j.bios.2021.113026

10. Kim TH, Hahn YK, Kim MS. Recent advances of fluid manipulation technologies in microfluidic paper-based analytical devices (μPADs) toward multi-step assays. *Micromachines (Basel)* (2020) 11(3):269. doi:10.3390/mi11030269

11. Mahmud MA, Blondeel EJM, Kaddoura M, MacDonald BD. Features in microfluidic paper-based devices made by laser cutting: how small can they Be? *Micromachines (Basel)* (2018) 9(5):220. doi:10.3390/mi9050220

12. Mansfield MA. The use of nitrocellulose membranes in lateral-flow assays. In: RC Wong, HY Tse, editors. *Drugs of abuse*. Springer (2005). p. 71–85. Available at: https://link.springer.com/book/10.1007/978-1-59259-951-6

13. Liu J. *Nitrate esters chemistry and Technology*. Singapore: Springer (2019).

14. Liu J. Nitrocellulose. In: *Nitrate esters chemistry and Technology*. Singapore: Springer (2019). p. 469–580. doi:10.1007/978-981-13-6647-5_10

15. Holstein CA, Chevalier A, Bennett S, Anderson CE, Keniston K, Olsen C, et al. Immobilizing affinity proteins to nitrocellulose: a toolbox for paper-based assay developers. *Anal Bioanal Chem* (2016) 408(5):1335–46. doi:10.1007/s00216-015-9052-0

16. Bangs Laboratories, Inc. Lateral flow tests: TechNote 303 web (2023). Available from: https://www.technochemical.com/bangs/img/TechNote%20303%20Web.pdf (Accessed August 20, 2023).

17. Cytiva. Membrane selection for lateral flow immunoassays - cytiva (2023). Available from: https://www.cytivalifesciences.com/en/us/solutions/lab-filtration/knowledge-center/Considerations-for-membrane-selection-for-lateral-flow-immunoassays (Accessed August 31, 2023).

18. Henderson D, White JC, Craighead HG, Adesida I. Self-developing photoresist using a vacuum ultraviolet F2 excimer laser exposure. *Appl Phys Lett* (1985) 46(9):900–2. doi:10.1063/1.95881

19. Skordoulis CD, Makropoulou MI, Serafetinides AA. Ablative etching of nitrocellulose with infra-red and ultra-violet laser radiation. *Opt and Laser Technol* (1995) 27(3):185–9. doi:10.1016/0030-3992(95)93639-9

20. Chang T-C, Molian PA. Excimer pulsed laser ablation of polymers in air and liquids for micromachining applications. *J Manufacturing Syst* (1999) 18(2):1–17. doi:10.1016/s1526-6125(99)70001-0

21. Nie J, Liang Y, Zhang Y, Le S, Li D, Zhang S. One-step patterning of hollow microstructures in paper by laser cutting to create microfluidic analytical devices. *Analyst* (2013) 138(2):671–6. doi:10.1039/c2an36219h

22. Mahmud MA, Blondeel EJM, Kaddoura M, MacDonald BD. Creating compact and microscale features in paper-based devices by laser cutting. *Analyst* (2016) 141(23):6449–54. doi:10.1039/c6an02208a

23. Kalish B, Tan MK, Tsutsui H. Modifying wicking speeds in paper-based microfluidic devices by laser-etching. *Micromachines (Basel)* (2020) 11(8):773. doi:10.3390/mi11080773

24. Spicar-Mihalic P, Toley B, Houghtaling J, Liang T, Yager P, Fu E. CO 2 laser cutting and ablative etching for the fabrication of paper-based devices. *J Micromech Microeng* (2013) 23(6):067003. doi:10.1088/0960-1317/23/6/067003

25. Hecht L. *Ultrakurzpuls-Laserprozesse für die Biosensor-Fertigung* (2024).

26. Hecht L, van Rossum D, Dietzel A. Femtosecond-laser-structured nitrocellulose membranes for multi-parameter Point-of-Care tests. *Microelectronic Eng* (2016) 158:52–8. doi:10.1016/j.mee.2016.03.020

27. Sumantakul S, Remcho VT. Selective laser ablation for *in situ* fabrication of enclosed channel porous-media microfluidic analytical devices. *Lab Chip* (2023) 23(14):3194–206. doi:10.1039/d3lc00208j

28. Urech L, Lippert T. Photoablation of polymer materials. In: *Photochemistry and photophysics of polymer materials*. John Wiley and Sons, Ltd (2010). p. 541–68.

29. Rethfeld B, Ivanov DS, Garcia ME, Anisimov SI. Modelling ultrafast laser ablation. *J Phys D: Appl Phys* (2017) 50(19):193001. doi:10.1088/1361-6463/50/19/193001

30. Bäuerle D. Thermal, photophysical, and photochemical processes. In: D Bäuerle, editor. *Laser processing and chemistry*. 4th ed. Berlin, Heidelberg: Springer (2011). p. 13–38. doi:10.1007/978-3-642-17613-5_2

31. Geertsen C, Briand A, Chartier F, Lacour J-L, Mauchien P, Sjöström S, et al. Comparison between infrared and ultraviolet laser ablation at atmospheric pressure—implications for solid sampling inductively coupled plasma spectrometry. *J Anal Spectrom* (1994) 9(1):17–22. doi:10.1039/ja9940900017

32. Yao L, Shi W, Qin J, Lin B. Fabrication and characterization of paper-based microfluidics prepared in nitrocellulose membrane by wax printing. *Anal Chem* 82:329–35. doi:10.1021/ac9020193

33. Schenk F, Weber P, Vogler J, Hecht L, Dietzel A, Günter G. Development of a paper-based lateral flow immunoassay for simultaneous detection of lipopolysaccharides of Salmonella serovars. *Anal Bioanal Chem* (2018) 410:863–8. doi:10.1007/s00216-017-0643-9

34. Sartorius. Unisart lateral flow (2024). Available from: https://www.sartorius.com/en/products/oem/oem-membranes-and-devices/diagnostic-membranes/unisart-lateral-flow (Accessed July 11, 2024).

35. Deutsch TF, Geis MW. Self-developing UV photoresist using excimer laser exposure. *J Appl Phys* (1983) 54(12):7201–4. doi:10.1063/1.331961

36. Geis MW, Randall JN, Deutsch TF, DeGraff PD, Krohn KE, Stern LA. Self-developing resist with submicrometer resolution and processing stability. *Appl Phys Lett* (1983) 43(1):74–6. doi:10.1063/1.94126

37. Furutani H, Fukumura H, Masuhara H, Kambara S, Kitaguchi T, Tsukada H, et al. Laser-induced decomposition and ablation dynamics studied by nanosecond interferometry. 2. A reactive nitrocellulose film. *J Phys Chem B* (1998) 102(18):3395–401. doi:10.1021/jp973459x